Modeling Next Generation Sensor Chips: Towards Predictive Band Structure Models for Quarternary III-V Semiconductor Alloys

Angus Gentles[1]* [2], Mohammad Dehghani[2], Rainer Minixhofer[1], Pedram Khakbaz[2] [3], Dominic Waldhör[2] and Michael Waltl[2]
[1]ams-OSRAM AG, Tobelbader Str. 30, 8141 Premstätten, Austria
[2]Institute of Microelectronics, TU Wien, 1040 Vienna, Austria
[3] Christian Doppler Laboratory for Single Defect Spectroscopy
*Email: angus.gentles@ams-osram.com

2024 International Conference on Simulation of Semiconductor Processes and Devices (SISPAD) | 979-8-3315-1635-2/24/$31.00 ©2024 IEEE | DOI: 10.1109/SISPAD62626.2024.10732909

***Abstract*—In this work, an *ab initio* scheme based on the DFT+U method is presented to model the electronic structure of ternary/quaternary semiconductor alloys. Within this method, optimal sets of Hubbard-U parameters are found for each binary compound of the alloy using a Bayesian optimization scheme. We introduce two interpolation schemes for the U parameters to describe the electronic structure in alloy supercells. By applying them on the InGaAsSb semiconductor alloy, we show that the predicted bandgap bowing is much closer to experimental data compared to results based on the virtual crystal approximation. The two schemes are shown to predict almost identical electronic bandgaps and provide a computationally efficient alternative to other approaches like the use of hybrid functionals.**

I. Introduction

Quaternary III-V semiconductor alloys such as InGaAsSb have been experimentally explored for decades [1]–[4] and are increasingly used in heterojunction device stacks, especially in short- and mid-wavelength infrared sensors. They provide widely tuneable bandgaps, allowing designers to choose appropriate absorption characteristics depending on the wavelengths of light being detected. Empirical interpolation schemes are frequently used in industry, specifically schemes developed by Vegard, Moon, Adachi or Donati [2], [5]–[7], to describe the material parameter variations within the composition space of semiconductor alloys. These schemes usually involve a simple linear interpolation between the binary semiconductors, plus a quadratic bowing term. However, there is only a limited understanding of the origin of these nonlinear bowing parameters. For instance, the scheme proposed by Littlejohn [8] is based on ternaries and that eventually used by Donati [7] is based on binaries. Since the different empirical interpolation schemes result in different weighting of the binary properties into the quaternary bowing parameter, a better theoretical understanding of these materials is required. This will reduce the amount of costly experiments in device stack development.

The lattice constants have been shown to be roughly linear with composition, while the electronic bandgap typically exhibit a far stronger bowing. Given that the bandgap is the most important physical quantity for photodetectors, and experimentally determining it for the multitude of different alloy compositions occurring in these devices is prohibitively expensive. This work aims at at a predictive *ab initio* scheme framework to model this property.

Unfortunately, *ab initio* modeling of binary semiconductors is very challenging, and modeling alloys is even more complex. Tight-binding calculations can accurately model the valence bands, but require many fitting parameters per atom [9]. Empirical pseudo-potentials have also been employed, but have similar problems of requiring many empirical parameters [10]. The obvious choice is then density functional theory (DFT). DFT is based on using the ground state electron density as the central quantity. It creates a fictional space of non-interacting electrons, the trace of which create the electron density. These are used to approximate the real electron eigenvalues, which are in turn used to model the higher states. All of the electron interaction is included in an exchange-correlation (XC) term, which currently has no analytic solution, but instead is approximated with (semi) local Local Density Approximation (LDA) and General Density Approximation (GGA) XC functionals [11]. DFT has several advantages over empirical pseudopotentials or tight-binding, such as requiring fewer empirical parameters. Ideally, it should use none, but the XC functionals introduce some approximation uncertainties again. XC functionals are often used to describe the atomic pseudopotentials, such as those developed for use with the PBE functional [11], an extensively used functional within the generalised gradient approximation. DFT has a good track record of reproducing lattice constants, bulk constants, and phonon spectra [12]. However, a major problem with DFT is that it systematically underestimates bandgaps. Indeed, of the four constituent binaries (InAs, GaAs, GaSb and InSb), only GaAs shows a bandgap at all when using (semi-)local functionals. Most commonly, this so-called bandgap problem is solved using hybrid functionals, such as HSE [13]. These hybrid functionals incorporate a part of the Hartree-Fock exchange interaction. Whilst producing well-shaped electronic bands with a finite bandgap, these hybrid functionals fail to predict the relative order of the bandgaps. Furthermore, they are prohibitively computationally expensive when it comes to the larger supercells required to accurately represent a semiconductor alloy.

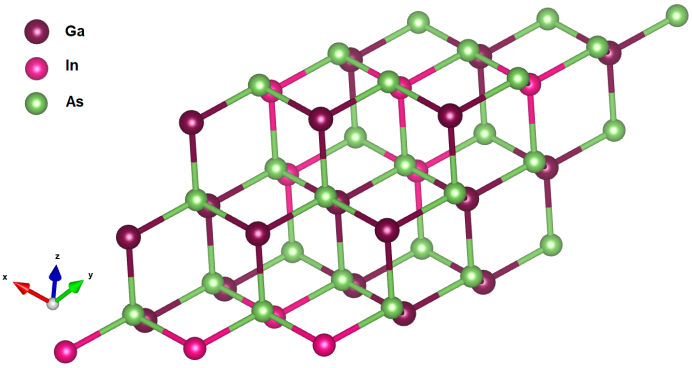

Fig. 1: An example of a $3 \times 3 \times 3$ supercell, with 54 atoms representing the random alloy $In_{0.33}Ga_{0.67}As$.

II. Methods

In this paper, we use a DFT+U approach as implemented in `QuantumESPRESSO` [14], [15] to model the bowing parameters of constituent ternary alloys within the InGaAsSb system, and then compare it to available experimental bowing values.

Rather than a standard GGA or LDA approach, we add Hubbard-U interactions [16] [to standard DFT], commonly known as the DFT+U method, to obtain correct band structures. This technique was initially developed for modelling the over-delocalisation of electrons in transition metals in d and f shells.

This was done using an electron self-interaction term for specified electron orbitals, specifically the valence p orbital. This tends to cause a greater localisation of the density of this electron around each atom. However, they have recently been used as an empirical parameter to improve band structure from standard (semi) local functionals, treated as an empirical correction to the XC functional. In this case, we are applying these to the p orbitals, as these were found to have the largest effect on the highest valence and lowest conduction bands.

We used a Bayesian optimization of the U parameters, with respect to the experimental parameters of the constituent binary band structures provided by Madelung [17]. Given the dependence of the U parameters on the local environment [19], we interpolated these parameters for supercells of ternary alloys using two different techniques labeled the *Local Interpolation Scheme* (LIS) and the *Global Interpolation Scheme* (GIS). The two schemes are used to predict the relation between the lattice constant and the bandgap of all ternary alloys as a function of the composition. We show that this approach leads to substantial improvement over the typically used virtual crystal approximation [18] (VCA) performed in a primitive unit cell.

A. Bayesian optimization of U parameters

A scheme similar to that used by Yu *et al.* [20] was employed to optimize the U parameters. Within Yu *et al.*, the HSE band structure is used to fit the valence and conduction bands, and the experimental bandgap. These two parts, the bandgap and the band shape differences, can be weighted, depending on which is more useful.

For comparison, we used band parameters from the experiment suggested by Madelung [17]. The first conduction band of these III-V alloys has a consistent shape, with an absolute minimum at the Γ point, and two more local minima at the L point and near the X point. These can be seen in the band structures in Fig. 3. The differences between the absolute minimum and the X and L minima in the brilluoin zone, defined as E_X and E_L, is averaged to find what has been labelled the 'bands difference'. The bandgap, E_G, was taken as the difference between the highest valence band at the Γ point and the absolute minimum of the first conduction band, which is always at the Γ point. For each proposed set of U parameters, a DFT calculation was carried out, involving a structural relaxation, then an non-self-consistent calculation to find the band structure. From this band structure, the conduction band minima were identified.

These were then inserted into the loss function shown in Equation 1. The α parameters are weighting parameters of the bandgap differences versus the valley differences. These were set to $\alpha_1 = 0.75$ and $\alpha_2 = 0.25$ in our optimization, as we wanted to prioritise the direct bandgap for its supercell bowing properties. ΔE_G, ΔE_X and ΔE_L are these values for this set of U parameters, and the experimental results from Madelung.

$$loss = -\left(\alpha_1 \Delta E_G^2 + \alpha_2 \left(\frac{\Delta E_L^2 + \Delta E_X^2}{2}\right)\right) \quad (1)$$

This loss function was then minimised using a Bayesian process. The loss function was fitted to a multi-dimensional Gaussian. An acquisition function is formed, which balances exploring new areas of the U parameters space, versus the expected maximum value of the function, allowing it to sample much of the space, whilst focusing mostly on the most likely improvements to the maximum of the function.

This sampling technique reduces the number of first-principles calculations required for finding optimal U parameters.

Scalar relativistic norm-conserving pseudopotentials [21] were used in these calculations, since they can also be employed in the Virtual Crystal Approximation (VCA), allowing for a direct comparison with our approach. A $12 \times 12 \times 12$ Monkhorst-Pack grid was used to sample the Brillouin zone of the primitive unit cell. The energy cutoff was set to 160 Ry.

B. Supercell calculations

Alloys were described using $3\times3\times3$ supercells as shown in Fig. 1 based on the 2-atom primitive cells using `sqsgen` [22]. Given the high temperature at which these alloys are typically grown, a completely random alloy was presumed, implying a minimal local correlation function.

In the LIS, a single atom type is characterised by its nearest neighbours. For instance, a type III atom, say In, might have n neighbouring As atoms, and $(4-n)$ Sb atoms, since all these semiconductor alloys crystallize in a Zincblende structure in which each atom has four nearest neighbours of the other type (III or V). In this case the U parameter would be calculated as $U_{\mathrm{In}} = (1-n)/4\ U_{\mathrm{In}}^{\mathrm{InAs}} + n/4\ U_{\mathrm{In}}^{\mathrm{InSb}}$, where $U_{\mathrm{In}}^{\mathrm{X}}$ represents the optimized U parameter for In in binary X.

In the GIS, the U parameters are combined for all atoms of each type on a global scale, considering the proportion of this type of atom in the entire alloy. For instance, if we were looking at In, in a mixture of 25% InAs and 75% InSb, the U parameter would be given by $U_{\mathrm{In}} = 0.25 U_{\mathrm{In}}^{\mathrm{InAs}} + 0.75 U_{\mathrm{In}}^{\mathrm{InSb}}$. One U parameter is thus assigned to each element independent of the local environment.

Supercell calculations are often compared to the much simpler VCA. This is a computationally simple method, where the two alloy pseudopotentials are linearly mixed, and then a primitive cell is calculated with these synthetic atoms. For more information, see Bellaiche [18] and references therein.

All supercell calculations were performed with a $4\times4\times4$ k-point grid to be commensurate with the k-mesh used for

the binary semiconductors and the VCA calculations done with a primitive unit cell. The energy cutoff was again 160 Ry for the SCF cycles and the subsequent ionic relaxations. For each ternary alloy, we considered two data points along the composition axis.

III. Results and Discussion

A. U parameter optimization

Samples of the loss function (dots) as well as the interpolating Gaussian Process (heatmap) are given for all binaries in Fig. 2. After initial exploration, the drawn samples start to cluster around an optimal point, indicating the convergence of the Bayesian optimization. The final U parameters for the binary compounds are provided in Fig. I. The resulting electronic and phononic band structures are shown in Fig. 3 and 4 for all binaries. As can be seen, there is a very good agreement with the experimental data taken from [17], [24], and [25], however, the optical phonons of of InAs are predicted to have lower values than are shown in experiment. InSb and GaSb are not included.

We observe that the fundamental bandgaps are most sensitive to changes in the U parameters for the group V p orbitals. In earlier tests, other orbitals were considered for the Hubbard correction, however, as they produced minimal changes to both the bandgap and the band shapes, they were discarded for a more condensed model. There appears to be a valley of lowest loss function values, where the bandgap is mostly converged, and along this valley, the other bands are changing shape.

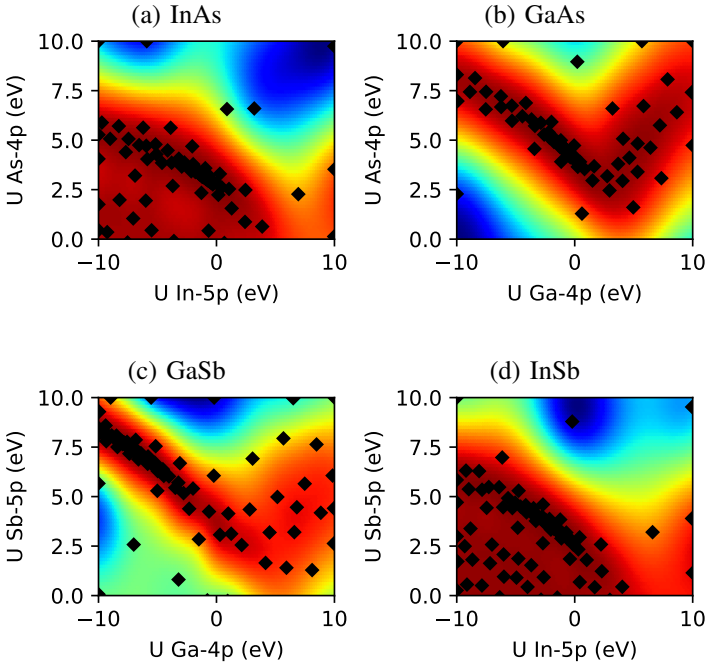

Fig. 2: Heatmaps for each binary, with the loss function on the z-axis, and the U parameters on the x- and y- axes

In Table I, several physical parameters are shown. Clearly, there is a vast improvement in the electronic bandgap. This is unsurprising, as the U parameters were optimized with respect to this bandgap. In the case of InAs and InSb, some deviation remains, due to deviation between Madelung [17] and Vurgaftman [23]. Our parameters were optimized with respect to Madelung, whereas the more

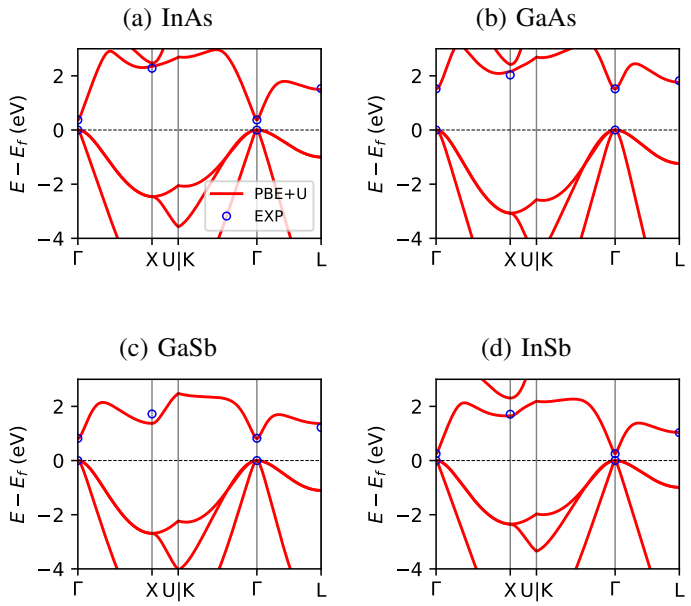

Fig. 3: Electronic band structures for every binary using their optimized U parameters.

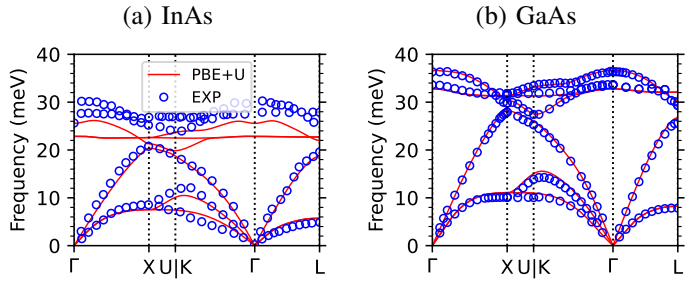

Fig. 4: Phononic band structures for InAs and GaAs using their optimized U parameters. The experimental data comes from [24] and [25].

reliable Γ-point data at 0K comes from Vurgaftman. However, Madelung includes data for L and X valleys for all binaries. In addition to this, though, the lattice constant a and the bulk modulus B also improve with respect to PBE. The smallest improvement shown is in the case of GaSb, possibly correlating to the comparatively high U parameters associated with it. The implication is that the band structure associated with PBE and that associated with the valleys at the positions given in Madelung are reasonably different.

B. Supercell bowing

When the optimized U parameters are applied to alloy supercells using the GIS and LIS methodologies, we find significantly more bowing and overall a better agreement with experimental values [7] compared to the VCA (see Fig. 5). This suggests some long-range interactions being present in alloy supercells which cannot be described within the VCA. However, the bowing is still underestimated compared to experiments, most evidently in the case of the Ga[As,Sb] ternary. It is also interesting to note that the bandgap bowing is almost the same for both schemes.

From the supercell calculations, it is also possible to map the band structures [26] back to the Brillouin zone

Binary	U (eV)		a (Å)			E_g (eV)			B (GPa)		
	III-p	V-p	PBE+U	PBE	EXP	PBE+U	PBE	EXP	PBE+U	PBE	EXP
GaAs	-0.70	4.43	5.63	5.75	5.65	1.52	0.55	1.52	83.6	72.1	75.3
InAs	-0.84	3.09	6.09	6.19	6.06	0.37	0.0	0.42	62.3	48.6	58.0
GaSb	-7.06	7.38	6.21	6.22	6.10	0.82	0.0	0.82	60.5	44.8	56.3
InSb	-1.84	3.48	6.48	6.63	6.48	0.25	0.0	0.22	47.3	37.1	57.7

TABLE I: Parameters produced by these U parameters, compared to experimental results and standard PBE. Experimental data was taken from [23] and the IOFFE website [27]

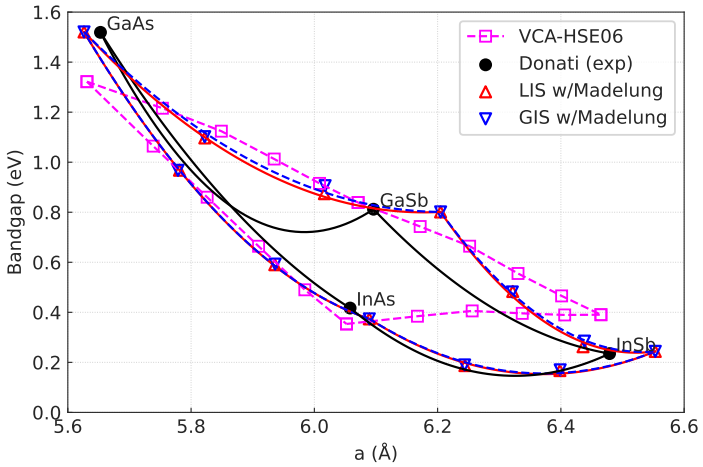

Fig. 5: A comparison of the VCA and our LIS and GIS approaches with experiments from Donati [7]. Overall, there is significant improvement over the VCA.

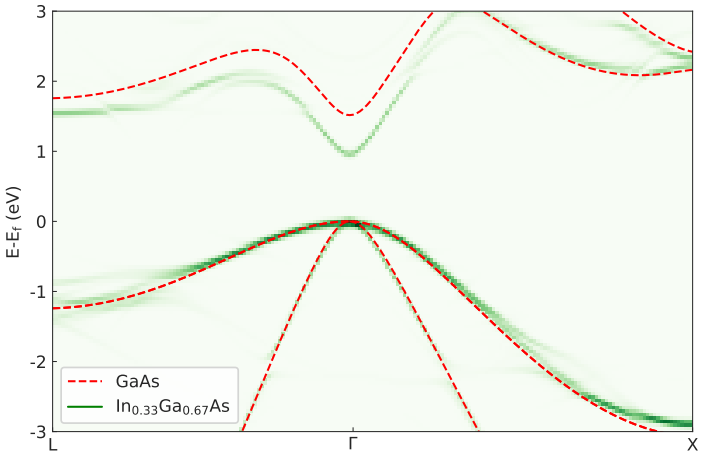

Fig. 6: Effective band structure of $In_{0.33}Ga_{0.67}As$ in green, with the band structure of GaAs overlaid in red for comparison.

of the primitive cell. Since the alloy breaks translational invariance, the electronic states are no longer exact Bloch eigenstates within the primitive cell, leading to smeared out bands, the so-called *effective band structure*, as shown in Figure 6. From this band structure, it is also possible to extract parameters such as the effective mass and the energies of the conduction band valleys at the X and L points in the Brillouin zone. Besides the different fundamental gap, the band structure strongly resembles its binary components, as the experimental values from Adachi [2] would indicate.

This band structure, whilst well defined at the Γ point, shows more alloy interference as the compound moves further from the respective binaries. However, there is no evidence of localised states in the bandgap. It is also worth noting that the bands are well defined around the Γ point, only later spreading out.

IV. Conclusions and Outlook

In this paper, we have presented a scheme for predicting bandgaps and band structures for quarternary alloys, applied to InGaAsSb. We used a Bayesian optimization scheme to find the U parameters for the binaries, and then used a local and global interpolation scheme to transfer these parameters to the alloy compounds, which were described using a supercell approach . This approach is computationally much more efficient compared to other techniques, such as the use of hybrid functionals. Using our method, we have found a substantial improvement over the almost linear relationship predicted by the VCA. However, further work is needed to identify the origin of the larger experimental bowing.

References

[1] S. Adachi, *J. Appl. Phys.* **53**, 8775–8792, 1982.
[2] S. Adachi, *J. Appl. Phys.* **61**, 4869–4876, 1987.
[3] D. Auvergne, J. Camassel, H. Mathieu, and A. Joullie, *J. Appl. Phys.* **35**, 133–140, 1974.
[4] Y. S. Kang *et al.*, *J. Appl. Phys.* **98**, 093714, 1974.
[5] R. L. Moon, G. A. Antypas, and L. W. James, *J. of El. Mat.* **3**, 635–644, 1974.
[6] L. Vegard, Zeitschrift für Kristallographie, **67**, 239–259, 1928
[7] G. Donati, R. Kaspi, and K. J. Malloy, *J. Appl. Phys.* **94**, 5814–5819, 2003.
[8] M. Littlejohn *et al.*, *Appl. Phys. Let.* **30**, 242–244, 1977.
[9] D. J. Chadi and M. L. Cohen, Physica Status Solidi (b), **68**, 405–419, 1975.
[10] J. R. Chelikowsky and C. L. Cohen, Phys. Rev. B, **14**, 554–582, 1976.
[11] J. Perdew, K. Burke, and M. Ernzerhof, *Phys. Rev. B*, **54**, 16533, 1996.
[12] G. Petretto *et al.*, Scientific Data, **5**, 2052–4463, 2018.
[13] A. P. Heyd, G. Scuseria, and M. Ernzerhof, *J. Chem. Phys.* **118**, 8207–8215, 2003.
[14] P. Giannozzi *et al.*, *J. Phys.: Cond. Mat.* **21**, 395502, 2003.
[15] P. Giannozzi *et al.*, *Phys. Rev. Let.* **29**, 465901, 2017.
[16] H. Kulik, *J. Chem. Phys.* **142**, 2015.
[17] O. Madelung, Semiconductors: Data Handbook, 2004.
[18] L. Bellaiche and D. Vanderbilt, Phys. Rev. B, **61**, 7877–7882, 2000.
[19] R. Tesch and P. M. Kowalski, Phys. Rev. B **105**, 195153, 2022.
[20] M. Yu, S. Yang, C. Wu and N. Marom, *npj Computational Materials* **6**, 2020.
[21] D. R. Hamann, Phys. Rev. B **88**, 085117, 2017.
[22] D. Gehringer, M. Friák, and H. Holec, *Comp. Phys. Comms.* **286**, 108664, 2023.
[23] I. Vurgaftman *et al.*, *J. Appl. Phys.* **89**, 5815–5875, 2001.
[24] D. Strauch and B. Dorner, J. Phys.: Condens. Matter **2**, 1457, 2004.
[25] N. Orlova, Physica Status Solidi (b), **119**, 541–546, 1983.
[26] V. Popescu and A. Zunger, *Phys. Rev. Let.* **104**, 236403, 2010.
[27] Ioffe Institute, Semiconductor Materials Parameters, Accessed: 2024-06-20.

V. Acknowledgements

The research leading to these results has received funding from the Austrian Research Promotion Agency FFG (project n895289).